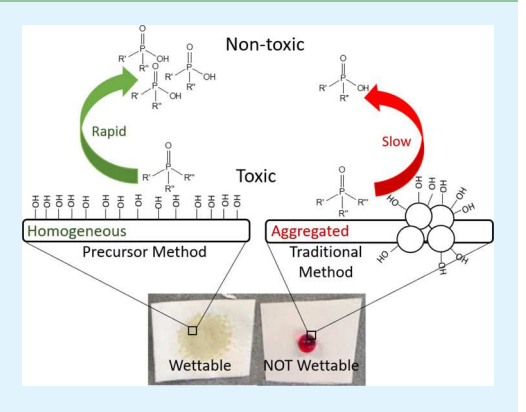


Metal Hydroxide/Polymer Textiles for Decontamination of Toxic Organophosphates: An Extensive Study of Wettability, Catalytic Activity, and the Effects of Aggregation

William E. Bernier, Jared B. DeCoste, and Wayne E. Jones, Jr*, Lo

Supporting Information

ABSTRACT: Electrospun nanofibers (NFs) incorporated with catalytically active components have gained significant interest in chemical protective clothing. This is because of the desirable properties of the NFs combined with decontamination capability of the active component. Here, a series of metal hydroxide catalysts $Ti(OH)_x$, $Zr(OH)_4$, and $Ce(OH)_4$ were incorporated into three different polymer NF systems. These new polymer/metal hydroxide composite NFs were then evaluated for their catalytic activity against a nerve agent simulant. Two methods were utilized to incorporate the metal hydroxides into the NFs. Method one used direct incorporation of Ti(OH)_{v1} Zr(OH)₄, and Ce(OH)₄ catalysts, whereas method two employed incorporation of Ti(OH)_x via a precursor molecule. Composite NFs prepared via method one resulted in greatly improved reaction rates over the respective pure metal hydroxides due to reduced aggregation of catalysts, with polymer/ Ce(OH)₄ composite NFs having the fastest reaction rates out of method one



materials. Interestingly, composite samples prepared by method two yielded the fastest reaction rates overall. This is because of the homogeneous distribution of the metal hydroxide catalyst throughout the NF. This homogeneous distribution created a hydroxyl-decorated NF surface with a greater number of exposed active sites for catalysis. The hydroxyl-decorated NF surface also resulted in an unexpected highly wettable composite NF, which also was found to contribute to the observed reaction rates. These results are not only promising for applications in chemical protective clothing but also show great potential for application in areas which need highly wettable membrane materials. This includes areas such as separators, antifouling membranes, and certain medical applications.

KEYWORDS: nanofibers, composites, metal hydroxide, wettability, CWAs, electrospinning, aggregation, water uptake

■ INTRODUCTION

Textiles both woven and nonwoven are used in every aspect of the modern day life. This ranges from clothing to filtration membranes, ¹⁻³ battery separators, ⁴⁻⁶ and certain medical applications. ⁷⁻⁹ Continued development of nanotechnology has allowed for vast improvements in the properties of these textiles. A technique known as electrospinning has shown significant interest for making these next-generation textile materials. This is because of the ease and simplicity of the technique to create nonwoven nanofibers (NF). 10 These NF materials have many desirable properties such as controllable porosity, high surface-to-volume ratio, and great particle protection. 11-13 Additionally, this technique has the advantage of easily incorporating active materials into the NFs to create a

multifunctional fabric. Because of this, electrospun composite NFs have shown great potential to improve current chemical/ biological (CB) protective clothing. CB protective clothing are designed to protect the wearer from exposure to chemical

Recent efforts by Ryu et al. explored using NF composites with laminated inner and outer layers for CB protective clothing. 14 The outer layer was made from a meta-aramid NF with MgO and POM as chemical absorbents, whereas the inner layer comprised Nylon 66 with the same absorbents.

Received: June 14, 2019 Accepted: August 1, 2019 Published: August 1, 2019



[†]Binghamton University State University of New York, 4400 Vestal Parkway East, Binghamton 13902, New York, United States

[‡]Department of Chemistry, Northwestern University, 2145 Sheridan Road, Evanston 60208, Illinois, United States

[§]State University of New York at Oswego, 7060 Route 104, Oswego 13126, New York, United States

US Army, Combat Capabilities Development Command Chemical and Biological Center, 5183 Blackhawk Road, Aberdeen Proving Ground 21010, United States

¹University of New Hampshire, 105 Main Street, Durham 03824, New Hampshire, United States

However, this clothing, like the current activated carbon-based CB clothing, only absorbs the agent leaving the clothing contaminated and dangerous. Because of this, significant effort has been focused on introducing catalytic activity to these CB protective clothing to greatly improve the safety of the clothing. Ying et al. showed the use of guanidine-functionalized Nylon 66 NFs to create a catalytically active NF fabric. 15 Their work showed successful decontamination of nerve agent simulant.

However, functionalization of NFs and other fabrics with metal-organic frameworks (MOFs) has dominated this area of CB protective clothing research in recent years. MOFs are a class of highly porous, adsorbent, and customizable crystalline materials.16 MOFs have been of high interest for these applications because of the ability of some of these MOFs to decontaminate chemical warfare agents (CWAs), both nerve and blister agents. 19-23 Several works have been reported showing successful incorporation of MOFs in NFs and other polymer supports. 24-32 These new multifunctional materials have decontamination ability toward simulant and nerve agents with potential for use in CB protective clothing applications. It is generally agreed that the active component in MOFs for hydrolysis of nerve agents, which are toxic organophosphates, are the metal nodes. Specifically, the exposed hydroxyl groups on the metal nodes.^{33,34} For zirconium-based MOFs such as UiO-66, UiO-66-NH₂, and NU-1000, the active sites are the zirconium hydroxide groups on the nodes.

Work done in 2012 by Peterson et al. showed that commercially available zirconium(IV) hydroxide (Zr(OH)₄) had rapid heterogeneous hydrolysis of nerve agents. However, since then, very little work has been carried out to explore using this metal hydroxide in NF composites for CB protective clothing application because of the advent of MOF research. In this work, Zr(OH)₄ was incorporated into different NF composites using electrospinning. This was done to understand the effects of incorporating metal hydroxide materials in NF systems for CB protective clothing application. The metal hydroxides, titanium hydroxide (Ti- $(OH)_x$) and cerium(IV) hydroxide (Ce(OH)₄) were also explored.

Additionally, three different polymer host systems were used to evaluate the effect of the polymer NF on the catalytic activity of the final composite. Polyvinylidene fluoride (PVDF), polymethylmethacrylate (PMMA), and polystyrene (PS) were used to make the polymer/M(OH)₄ composite NFs. Finally, two different incorporation methods of Ti(OH)_x were used to make the polymer/Ti(OH)_x composite NFs. In method one, Ti(OH)_x powder was added directly to the polymer solution step of the NF fabrication before electrospinning. This is identical to the incorporation method for polymer/Zr(OH)₄ and polymer/Ce(OH)₄ composites. In the second method, a precursor molecule of Ti(OH)x, titanium-(IV) isopropoxide (TTiP), was added to the polymer solution before electrospinning. When electrospun, the TTiP will spontaneously hydrolyze to Ti(OH), from reaction with water in the air. These two incorporation methods will be compared to determine the effects on the properties of the final composite.

It is predicted that Ce(OH)₄ and its corresponding composite NFs will have the fastest reaction rates. This is because of the known 4f-orbital contribution of the Ce(IV), which has been shown to give it significantly improved hydrolysis rates for organophosphates. 36 Additionally, CeMOFs have been shown to outperform Zr-MOFs for the same reason.³³ Zr(OH)₄ and its corresponding composite NFs are likely to follow Ce(OH)₄. This is because of the complex surface chemistry of Zr(OH)₄ which has been shown to give it rapid catalytic hydrolysis toward organophosphates.³⁵ reports have been found using Ti(OH), for organophosphate hydrolysis, and so its rate cannot be predicted.

■ RESULTS AND DISCUSSION

The metal hydroxides, (M(OH)₄), Ce(OH)₄, and Zr(OH)₄ are available commercially. However, Ti(OH)_r is not and must be synthesized in-house from titanium(IV) isopropoxide (TTiP). The synthesis was performed using a modified procedure from Yuan et al.³⁷ Before fabricating the polymer/ M(OH)₄ composites, the chemical composition of the synthesized $Ti(OH)_x$ was verified. The composition of the commercially available Ce(OH)₄ and Zr(OH)₄ were also confirmed.

Powder X-ray diffraction (PXRD) was performed on the samples and showed no significant crystal structure for both $Ti(OH)_x$ and $Zr(OH)_4$, Figure S2. This is consistent with the primarily amorphous structure of the Zr(OH)₄ reported in the past, which also suggests that Ti(OH)_r is predominantly amorphous.³⁵ On the other hand, Ce(OH)₄ does show significant crystal structure. Diffuse reflectance infrared spectroscopy (DRIFTS) of Ti(OH)_x, Zr(OH)₄, and Ce(OH)₄ show broad alcohol stretches at 3300 cm⁻¹, Figure S3. This is from the hydroxyl group bound to the metal because all of the physisorbed water was removed prior to the measurement. A peak at 1037 cm⁻¹ is present in the DRIFTS spectrum of Ce(OH)₄ and is a result of Ce-O stretching. This is not observed for Zr(OH)₄ and Ti(OH)_r because they are expected to appear closer to 600 cm⁻¹, which is below the cut-off for the spectrum. Peaks from hydrogen-oxygen-hydrogen stretches $(\sim 1650 \text{ cm}^{-1})$ were present for all three metal hydroxides and can be used as an indicator for the presence of the metal hydroxides in the respective polymer/M(OH)₄ composites. Raman spectra of the three metal hydroxides in Figure S4 show signals from 50 to 1050 cm⁻¹ corresponding to the M-O vibrations. The broad Ti-O signals suggest poor crystallinity of the $Ti(OH)_x$ structure, which is in good agreement with the PXRD. Thermal analysis of the metal hydroxides shows significant mass loss for all metal hydroxides beginning around 80-100 °C, Figure S5. Mass spectrometry analysis shows that this major mass loss is due to water, likely from both absorbed water and loss of water from conversion of the metal hydroxides to their respective metal oxides.

Potentiometric acid-base titration experiments have been used in the past to evaluate the pK_a environments of both MOFs and metal hydroxides, which can give insight to the reactivity of the material. 35,38 Here, potentiometric acid-base titrations were performed on Ti(OH)x, Zr(OH)4, and Ce(OH)₄ by keeping the total moles of metal hydroxides consistent. The titration for each metal hydroxide is shown in Figure S6. The p K_a for Ti(OH)_a, Zr(OH)₄, and Ce(OH)₄ are 3.4, 4.8, and 3.9, respectively. However, these materials are known for having multiple pK_a environments.³⁴ Both Zr(OH)₄ and Ce(OH)₄ showed one single inflection point at a pH of 7.51 and 7.26. $Ti(OH)_x$ appears to have two inflection points with the major inflection point occurring at a pH of 4.69 and the minor inflection point occurring at 8.6.

Finally, the surface area (SA) of the different metal hydroxides was evaluated using N₂ isotherm measurements. First, adsorbed water was removed by degassing the samples at either 60 or 120 °C before the N2 isotherm experiments. PXRD was also taken after both activation temperatures to determine if there is any change in the structure from metal oxide formation. The N₂ isotherms for the metal hydroxides are shown in Figure 1 with the Brunauer-Emmett-Teller

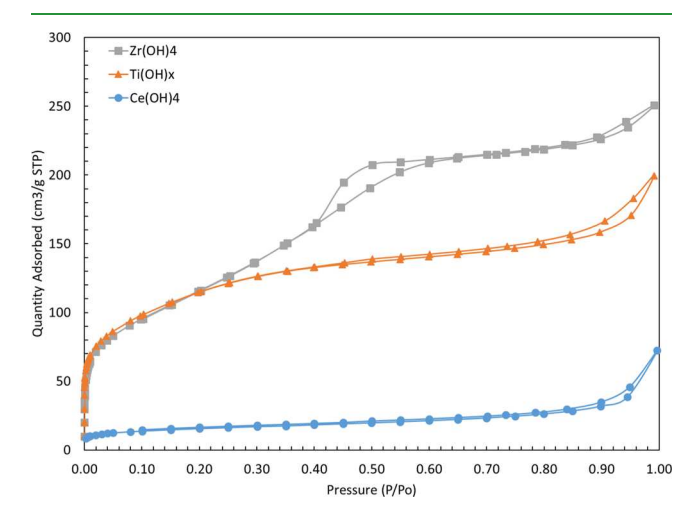


Figure 1. N₂ isotherms of metal hydroxides degassed at 60 °C.

(BET) SA shown in Table S1. All samples showed about a 10% decrease in SA at the higher activation temperature of 120 °C. The PXRD does not show any additional diffraction peaks arise from the formation of metal oxide, Figure S7. The BET SA of Zr(OH)₄ was 441 cm³/g, which is consistent with the literature.³⁹ Ti(OH)_x also had a SA comparable to Zr(OH)₄ with 414 cm³/g, whereas Ce(OH)₄ had a low SA of 56 cm³/g.

With the metal hydroxides, fully characterized polymer/ M(OH)₄ NF composites were made using electrospun PVDF, PMMA, and PS. A sample was made for each combination of polymer and metal hydroxide. For clarity, polymer/Ti(OH), composite NFs prepared using method two will be designated as polymer/TTiP. The polymer/M(OH)₄ composites are first characterized with DRIFTS and Raman spectroscopy. DRIFTS of all three polymer sets showed that the pure polymer NF spectra was very similar to the respective polymer composite spectra, with O-H (~3301 cm⁻¹) and H-O-H (~1614 cm⁻¹) signals emerging for samples with a metal hydroxide, Figures 2-4. Interestingly, there were a few significant differences between the composite and the pure polymer NFs for the PVDF and PS samples. For the PS sample set, the strong peak at 679 cm⁻¹ is characteristic for ring deformation of the phenyl group in the PS, Figure 2. When incorporating a metal hydroxide into the composite NF, the signal increases with respect to the molar loading of the metal hydroxide. Samples with the highest molar loading of the metal hydroxide, PS/Ti(OH)_r and PS/TTiP, had the strongest ring deformation signal. This indicates that incorporation of metal hydroxides into the PS NF distorts the polymer structure.

A similar phenomenon is seen with the PVDF composite samples. When incorporating metal hydroxides into the PVDF NF, two distinct signals emerge at 1496 and 1450 cm⁻¹, Figure 3. These signals are identified as CH₂ deformation, which again suggests that incorporation of metal hydroxides results in a deformed polymer structure. Evidence of polymer deformation is not observed in the PMMA samples and is likely due to the strong C=O and CH3 signals in the region where the CH2

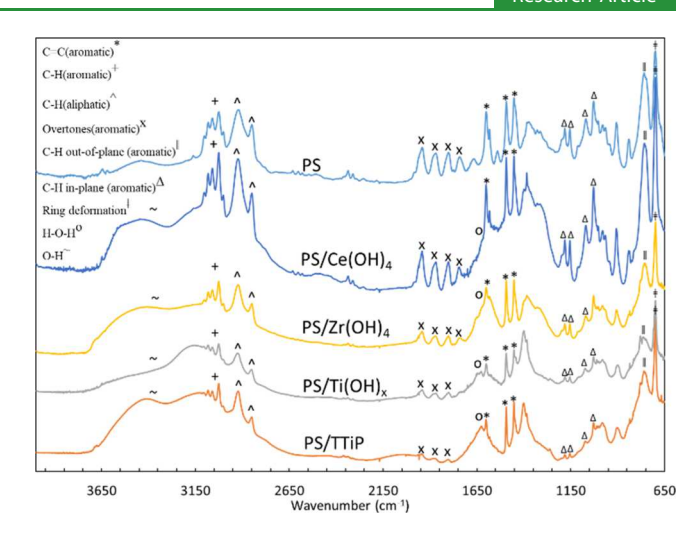


Figure 2. DRIFTS of PS/M(OH)₄ composite NFs.

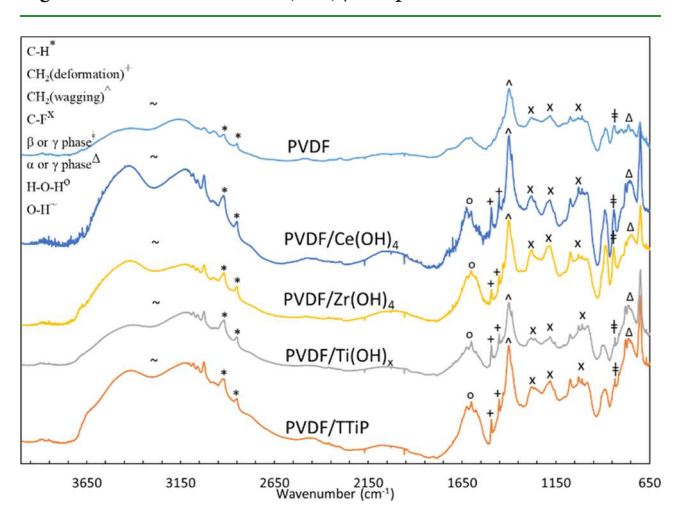


Figure 3. DRIFTS of PVDF/M(OH)₄ composite NFs.

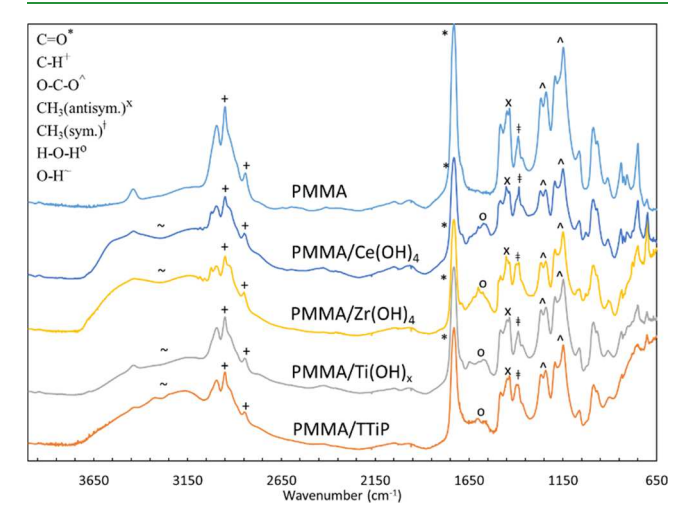


Figure 4. DRIFTS of PMMA/M(OH)₄ composite NFs.

deformation would occur, Figure 4. The Raman spectra of the different polymer/M(OH)₄ composites did not show evidence of polymer deformation but did show evidence of the presence of a metal hydroxide for PVDF/Ce(OH)₄, PVDF/Zr(OH)₄, PMMA/Ti(OH), PMMA/TTiP, PMMA/Ce(OH), PMMA/ $Zr(OH)_4$, and $PS/Ce(OH)_4$ samples, Figures S8–10.

Scanning electron microscopy (SEM) was performed on each set of samples to determine what effect(s) the incorporation of a metal hydroxide has on the morphology of the respective polymer NF. The SEM images of the pure PVDF, Figure 5, PMMA, and PS NFs, Figure S11, show

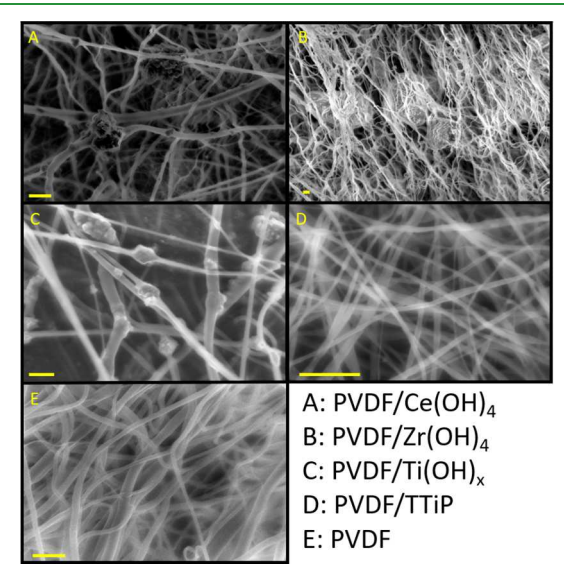


Figure 5. SEM images of PVDF/M(OH)₄ composites. Scale bars are at 1 μ m.

relatively smooth morphology with no aggregation. When incorporating Ti(OH)_x, Zr(OH)₄, and Ce(OH)₄ into each respective polymer, significant aggregation is present in the NFs. The average diameter of the PMMA and PS composite samples appears to increase as well with the incorporation of $Zr(OH)_4$ and $Ce(OH)_4$. As for the polymer composites incorporated with TTiP, no aggregation is present in the SEM. This indicates that the distribution of Ti(OH), in the NFs for method two results in a uniform distribution of $Ti(OH)_x$ with no aggregation.

Next, both the thermal stability and mass loading of the metal hydroxides were evaluated using thermogravimetric analysis (TGA). TGA experiments were performed under O₂ with N₂ protective gas and a heating ramp of 20 °C per minute up to 800 °C. The remaining mass after heating is the metal

oxide formed from the respective metal hydroxide. This can then be back calculated to determine the total mass of the metal hydroxide in the polymer composite sample. The TGA of the polymer/M(OH)₄ composite samples are shown in Figure S12. No clear trend can be deciphered from the thermal analysis of the different polymer/M(OH)₄ using Ti(OH)_x, Zr(OH)₄, and Ce(OH)₄. On the other hand, the polymer/ TTiP samples all showed consistent decreases in thermal stability. It is unclear as to the reason why incorporating of Ti(OH), via method two results in reduced thermal stability. But it is likely linked to the homogeneous distribution of $Ti(OH)_r$ in the NFs.

Table S2 shows the mass loading of metal hydroxides in each of the polymer composites calculated from the TGA. The theoretical weight percent for each of the samples is 44.9. However, the fabrication process causes some variation in the amount incorporated. This may be due in part by the aggregation seen with the metal hydroxides incorporated as a powder as suggested in TGA experiments performed by Peterson et al. with MOF systems.4

After full characterization of the metal hydroxides and their respective polymer/M(OH)₄ composite NFs, the catalytic activity of these samples was evaluated. The catalytic activity was evaluated using a well-known procedure with a nerve agent simulant, O,O-dimethyl O-(4-nitrophenyl) phosphate (DMNP).⁴¹ Each degradation experiment was performed in triplicate, and the half-lives are shown in Table 1 and Figure 6 with percent conversion plots in Figure S13. The reaction rates achieved for the Ti(OH)_x, Zr(OH)₄, and Ce(OH)₄ powders where 1430, 484, and 183 min half-lives respectively. Zr(OH)₄ reactivity toward VX nerve agents has shown rapid decontamination in the past for a reaction without buffer.³⁵ However, in this case, in a buffered solution against the CWA simulant, DMNP, the reaction is slow.

 $Ti(OH)_x$ had a comparable SA to $Zr(OH)_4$, which suggests that the p K_a of Ti(OH)_x plays a significant role in the observed catalytic activity. $Ce(OH)_4$ had both a low p K_a and BET SA. This suggests that the rate of DMNP hydrolysis for Ce(OH)₄ should be lower than that for Zr(OH)4, but the opposite is observed. These results support the original hypothesis that the Ce(OH)₄ would have the fastest reaction rate because of the known contribution of the 4f-orbitals and in fact appears to be the primary reason for its high reactivity. 33,36

Table 1. DMNP Half-Lives Using M(OH)₄ and Polymer/M(OH)₄ Composite Samples with Both Calculated (Theoretical) and Measured (TGA) mol Loadings of Catalyst

	O,O-dimethyl O-(4-nitrophenyl) phosphate (DMNP) half-lives (min.)			
$Ce(OH)_4$	183 ± 25	52 ± 19	105 ± 25	157 ± 40
measured	N/A	(24.9 μ mols)	(24.7 μ mols)	$(19.0 \ \mu \text{mols})$
calculated	(46.6 μ mols)	$(25.9 \ \mu \text{mols})$	$(25.9 \ \mu \text{mols})$	$(25.9 \ \mu mols)$
$Zr(OH)_4$	484 ± 19	184 ± 11	207 ± 16	303 ± 26
measured	N/A	(26.6 μ mols)	$(32.3 \ \mu \text{mols})$	$(28.6 \ \mu \text{mols})$
calculated	(46.6 µmols)	$(33.9 \ \mu \text{mols})$	$(33.9 \ \mu \text{mols})$	$(33.9 \ \mu mols)$
$Ti(OH)_x$	1430 ± 227	724 ± 30	630 ± 0	891 ± 172
measured	N/A	$(38.0 \ \mu \text{mols})$	$(36.4 \mu mols)$	$(52.3 \ \mu \text{mols})$
calculated	(46.6 μ mols)	(46.6 μ mols)	(46.6 μ mols)	(46.6 μ mols)
TTiP	N/A	135 ± 8	52 ± 13	40 ± 3
measured	N/A	(40.7 μ mols)	$(55.1 \ \mu \text{mols})$	(51.1 μmols)
calculated	(46.6 μ mols)	(46.6 μ mols)	(46.6 μ mols)	(46.6 μ mols)
		2310	6931	3466
		PVDF	PMMA	Polystyrene

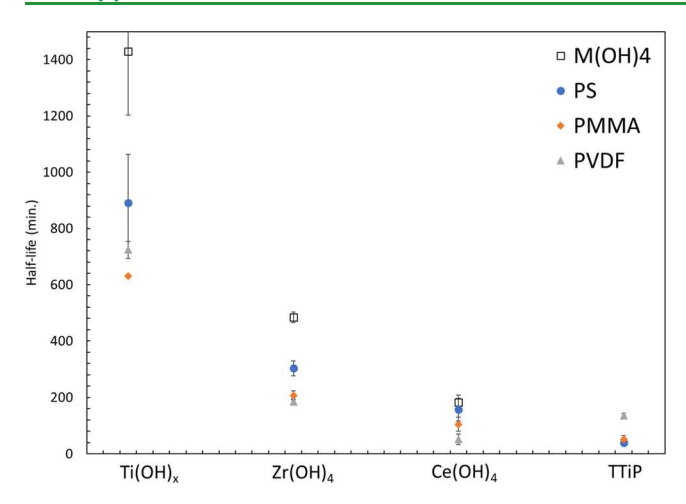


Figure 6. Plot of half-lives vs metal hydroxide with their respective polymer composites.

Incorporation of $Ti(OH)_{x}$, $Zr(OH)_4$, and $Ce(OH)_4$ into polymer NFs of either PVDF, PMMA, or PS showed vast improvements in catalytic activity for all of the polymer/ M(OH)₄ combinations. The activity of Ti(OH)_x improved from a half-life of 1430 to 724, 630, and 891 min for PVDF, PMMA, and PS, respectively. Zr(OH)₄ improved from 484 to 184, 207, and 303 min for PVDF, PMMA, and PS. Finally, Ce(OH)₄ improved from 183 to 52, 105, and 157 min for PVDF, PMMA, and PS. The significant improvements seen when incorporating metal hydroxides into a polymer NF is attributed to the improvement in distribution of the metal hydroxide, minimizing the amount of aggregation and exposing more active sites. It is also important to note that for both the polymer/ $Zr(OH)_4$ and polymer/ $Ce(OH)_4$ composite NFs, the amount of active catalyst used in the degradation experiment was less than that used for the pure metal hydroxide experiments. And yet, the reactions achieved are still significantly faster.

Each of the different sets of polymer/M(OH)₄ composites showed the same trend as the powder metal hydroxides with polymer/Ti(OH), composites having the slowest rate followed by polymer/Zr(OH)₄, and polymer/Ce(OH)₄ composites having the fastest rate of hydrolysis, Figure 6. Interestingly, it was found that the polymer used does affect the reaction rate of the final polymer/M(OH)₄ composite. The PS/M(OH)₄ composites were shown to have the slowest reaction rate out of the three polymer systems followed by PMMA/M(OH)₄. The PVDF/M(OH)₄ composites overall had the fastest reaction rates for Ti(OH)_x, Zr(OH)₄, and Ce(OH)₄ composites. The one exception to this trend is with the PMMA/Ti(OH)_x composite, which is the fastest of the trio of samples. Surprisingly, the polymer/TTiP samples achieved half-lives of 135, 52, and 40 min for PVDF/TTiP, PMMA/TTiP, and PS/ TTiP, respectively. These rates were even faster than most polymer/Ce(OH)₄ samples.

To better understand the trends observed using the different polymer systems as well as explain the rapid rates achieved for the polymer/TTiP composites, the wettability of the polymer/M(OH)₄ samples were evaluated. Water contact angle measurements were performed first and showed that PVDF, PMMA, and PS polymer NFs were all hydrophobic with contact angles around 140°, Table S3 and Figures 7 and S14. Incorporation of the metal hydroxides, Ti(OH)_x, Zr(OH)₄, and Ce(OH)₄ did not show any significant change in the

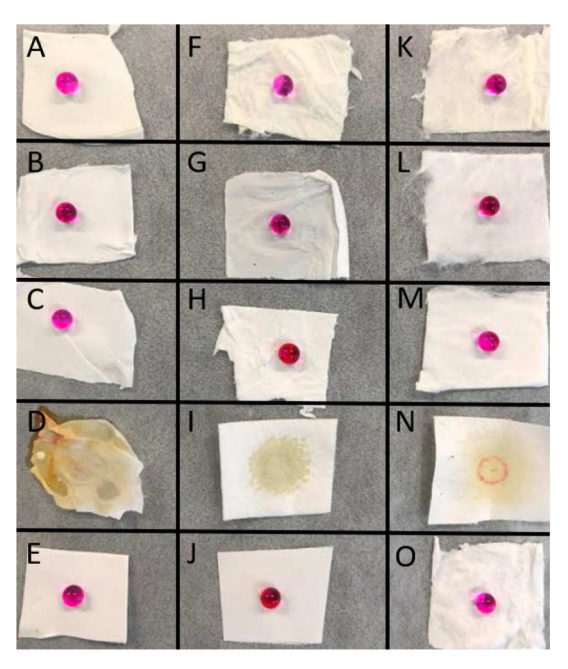


Figure 7. Pictures of water wetting extents of PVDF (E), PVDF/TTiP (D), PVDF/Ti(OH) $_x$ (C), PVDF/Zr(OH) $_4$ (B), PVDF/Ce(OH) $_4$ (A), PMMA (J), PMMA/TTIP (I), PMMA/Ti(OH) $_x$ (H), PMMA/Zr(OH) $_4$ (G), PMMA/Ce(OH) $_4$ (F), PS (O), PS/TTIP (N), PS/Ti(OH) $_x$ (M), PS/Zr(OH) $_4$ (L), and PS/Ce(OH) $_4$ (K) samples with added color for contrast.

contact angle from the pure polymer NF. Interestingly, the polymer/TTiP samples all showed complete wetting by contact angle measurements. Complete wetting via contact angle measurements for PVDF/TTiP NFs was reported before by our group but a comprehensive study explaining the reasons for the improved wetting and its effects on the catalytic activity has not been performed before. The complete and rapid wetting explains the fast reaction rates observed for the polymer/TTiP samples. This rapid wetting allows both DMNP and water to penetrate and saturate all active sites on the surface and within the composite resulting in the fast rates observed.

Although the water contact angle measurements explain the fast rates achieved for the polymer/TTiP samples, they do not explain the observed trends between different polymer systems. To further evaluate the wettability of the different polymer systems, water uptake measurements were performed. This was performed using a modified procedure for evaluating electrolyte uptake of battery separators. 43,44 The measurements were taken after 2 h of soaking. The first trial showed water uptakes of 577, 346, and 149% for PVDF, PMMA, and PS, respectively, Table S4. This supports the trends observed between the PVDF/M(OH)₄, PMMA/M(OH)₄, and PS/M(OH)₄ composites in the DMNP experiments. However, trials two and three do not follow this trend. This is potentially due to the use of different batches between trials. Regardless, further wetting tests will be necessary to support the polymer wettability hypothesis for the trends observed.

The complete wetting and fast reaction rates observed with the polymer/TTiP composites are explained by the homogeneous distribution of $Ti(OH)_x$ in the NFs. This very uniform distribution is hypothesized to result in the surfaces of the respective polymer NFs being decorated uniformly by the hydroxyl groups of $Ti(OH)_x$, Figure 8. This gives the polymer

the high-surface energy seen in the wetting experiments as well as fast reaction rates.

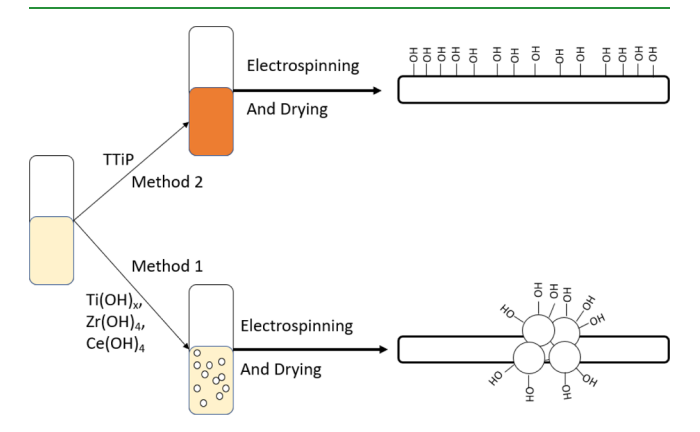


Figure 8. Illustrations of polymer/TTiP surface with uniform distribution of hydroxyl groups compared to the polymer/Ti(OH)_x surface with nonuniform hydroxyl distribution.

The rapid reaction rates achieved are due to vast numbers of hydroxyl active sites being available on the surface of the polymer. Additionally, the rapid wetting allows for DMNP simulant to easily penetrate the surface of the polymer and react with any additional active sites imbedded within the polymer composite NF. However, this does not explain the differences in reaction rates between PVDF/TTiP and the other two polymer/TTiP systems. The significant differences are attributed to the dispersion of the polymer/TTiP composite in the degradation experiment. Both the PMMA/ TTiP and PS/TTiP form a slurry when added to the aqueous buffer solution but the more physically durable PVDF/TTiP retains its structure and does not form a slurry, Figure 9.

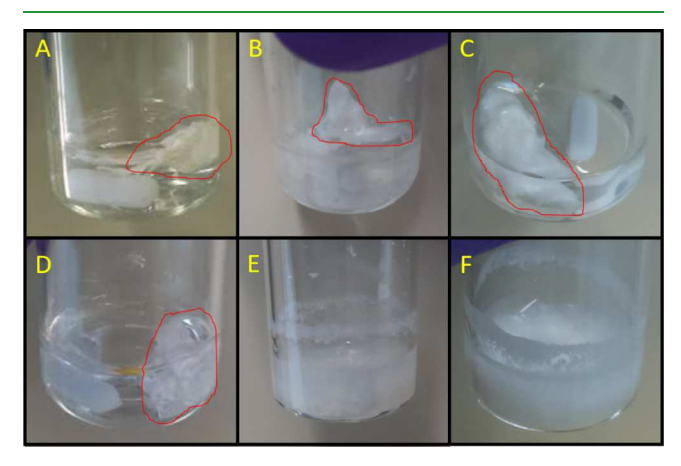


Figure 9. Pictures of PVDF/TTiP (A), PMMA/TTiP (B), and PS/ TTiP (C) before stirring and PVDF/TTiP (D), PMMA/TTiP (E), and PS/TTiP (F) after stirring for 30 min in aqueous buffer solution.

The slurry formed by PMMA/TTiP and PS/TTiP is directly related to the physical durability of the PMMA and PS NFs. Both polymer NFs are very fragile and can tear easily. When combined with the improved wettability, the buffer can penetrate the material and allow for swelling and eventually disintegration of the polymer composites. On the other hand, PVDF NFs are very durable and can easily retain their structure when swollen with the buffer. Therefore, the faster reaction rates by the PMMA/TTiP and PS/TTiP are because

of the ability of the two composites to form a slurry in solution. This allows for a more uniform distribution of the catalyst in the degradation experiment, resulting in faster observed rates.

CONCLUSIONS

This work has demonstrated a fundamental and comprehensive study of the catalytic hydrolysis of a nerve agent simulant using the metal hydroxides, Ti(OH)_x, Zr(OH)₄, and Ce(OH)₄ incorporated in different polymer composite NFs. It has been demonstrated that the difference in activity between polymer/ $Ti(OH)_x$ and polymer/ $Zr(OH)_4$ composites is related to a combination of both pKa and SA of the respective metal hydroxides, with the lower p K_a and SA of Ti(OH)_x resulting in a slower reaction rate than the Zr(OH)4. However, for polymer/Ce(OH)₄ composites, fast rates were achieved because of the well-known ability for Ce(IV) to utilize its 4forbitals in the reaction. This has been shown in the past by Shigekawa et al. for a homogeneous system and Islamoglu et al. for a heterogeneous system with Ce-MOFs. 33,3

Incorporation of these metal hydroxides into polymer NFs using method one was shown to greatly improve the catalytic rate of the polymer/M(OH)₄ composite compared to the pure metal hydroxide. This was due to decreased aggregation of the respective metal hydroxide in the NFs. PVDF/Ce(OH)₄ composites had the fastest reaction rates out of the method one materials and therefore have the greatest potential out of the series. Interestingly, the fastest decontamination rates were not achieved by the polymer/Ce(OH)₄ composites as one would expect from the decontamination tests with the pure metal hydroxides. But rather with the composites incorporated with Ti(OH), via method two using the precursor molecule TTiP. The incorporation of TTiP during the polymer solution step resulted in a homogeneous distribution of Ti(IV) within the polymer solution. This homogeneous distribution of Ti(IV) is seen in the final composite after electrospinning. After hydrolysis, the TTiP forms a homogeneously distributed $Ti(OH)_x$ with no observed aggregation. This homogeneous distribution results in a uniform distribution of catalytically active hydroxyl groups over the surface of the composite NF giving it improved reaction rates.

Additionally, the uniform hydroxyl coverage created a highly wettable material. The greatly improved wettability is hypothesized to contribute to the enhanced reaction rates as well. This is because of the improved ability of simulant and water to penetrate further into the materials and gain access to more active sites. Finally, although these new polymer/TTiP composite NF materials show rapid reaction rates for simulant hydrolysis, there are some disadvantages. The PS/TTiP and PMMA/TTiP composite NFs could not be used in CB protective clothing due to the poor physical integrity of the material. On the other hand, PS/TTiP and PMMA/TTiP could be used as a cheap method for decontaminating stockpiles of CWA. Because of the great structural integrity, fast reaction rates, and great wettability the PVDF/TTiP composite, it has the greatest potential for use in protective clothing from the method two material.

This method for creating highly wettable composite NFs has many other potential applications and is likely not limited to TTiP precursor materials. It is speculated that other precursor molecules like TTiP can be used to generate a homogeneous solution prior to electrospinning and convert to the final catalyst after electrospinning. Currently, this new method allows fabrication of completely wettable membranes using

essentially any polymer of choice. This eliminates restrictions to certain polymer materials based on wettability. It has great separators, ^{50–52} biodegradable plastics, ⁵³ and certain medical applications. ^{54,55}

ASSOCIATED CONTENT

Supporting Information

The Supporting Information is available free of charge on the ACS Publications website at DOI: 10.1021/acsami.9b10440.

Experimental procedures, SEM, PXRD, DRIFTS, Raman, TGA, potentiometric titrations, BET SA, DMNP percent conversion, water contact angle, and water uptake (PDF)

AUTHOR INFORMATION

Corresponding Author

*E-mail: wayne.jones@unh.edu.

ORCID ®

Derek B. Dwyer: 0000-0003-4614-4264

Jian Liu: 0000-0002-5024-1879

Jared B. DeCoste: 0000-0003-0345-2697 Wayne E. Jones, Jr: 0000-0002-4519-051X

Notes

The authors declare no competing financial interest.

ACKNOWLEDGMENTS

We acknowledge funding from the Army Research Office (ARO) W911NF1310235 as well as the Joint Science and Technology Office for Chemical Biological Defense (JSTO-CBD) under contract BA13PHM210 at the Edgewood Chemical Biological Center. This experimental work has been carried out with support from the Department of Chemistry at Binghamton University, State University of New York. This work was supported as part of the Multidisciplinary GAANN in Smart Energy Materials, a Graduate Areas of National Need, funded by the U.S. Department of Education, under award #P200A150135. This work was also supported under the NSF REU program award #DMR-1658990.

■ REFERENCES

- (1) Jabur, A. R.; Abbas, L. K.; Moosa, S. A. Fabrication of Electrospun Chitosan/Nylon 6 Nanofibrous Membrane toward Metal Ions Removal and Antibacterial Effect. Adv. Mater. Sci. Eng. 2016, 2016, 1-10.
- (2) Yoon, K.; Hsiao, B. S.; Chu, B. Formation of Functional Polyethersulfone Electrospun Membrane for Water Purification by Mixed Solvent and Oxidation Processes. Polymer 2009, 50, 2893-
- (3) Ma, H.; Burger, C.; Hsiao, B. S.; Chu, B. Ultra-fine Cellulose Nanofibers: New Nano-scale Materials for Water Purification. J. Mater. Chem. 2011, 21, 7507-7510.
- (4) Elia, G. A.; Ducros, J.-B.; Sotta, D.; Delhorbe, V.; Brun, A.; Marquardt, K.; Hahn, R. Polyacrylonitrile Separator for High-Performance Aluminum Batteries with Improved Interface Stability. ACS Appl. Mater. Interfaces 2017, 9, 38381-38389.
- (5) Hou, J.; Jang, W.; Kim, S.; Kim, J.-H.; Byun, H. Rapid Formation of Polyimide Nanofiber Membranes via Hot-press Treatment and their Performance as Li-ion Battery Separators. RSC Adv. 2018, 8, 14958-14966.
- (6) Li, H.; Zhang, B.; Lin, B.; Yang, Y.; Zhao, Y.; Wang, L. Electrospun Poly(ether ether ketone) Nanofibrous Separator with

- Superior Performance for Lithium-Ion Batteries. J. Electrochem. Soc. 2018, 165, A939-A946.
- (7) Li, Z.; Zhou, P.; Zhou, F.; Zhao, Y.; Ren, L.; Yuan, X. Antimicrobial eugenol-loaded electrospun membranes of poly(Ecaprolactone)/gelatin incorporated with REDV for vascular graft applications. Colloids Surf., B 2018, 162, 335-344.
- (8) Qu, Y.; Wang, B.; Chu, B.; Liu, C.; Rong, X.; Chen, H.; Peng, J.; Qian, Z. Injectable and Thermosensitive Hydrogel and PDLLA Electrospun Nanofiber Membrane Composites for Guided Spinal Fusion. ACS Appl. Mater. Interfaces 2018, 10, 4462-4470.
- (9) Yang, S. B.; Yeum, J. H. Morphological Comparison of Aligned Poly(vinyl alcohol) Nanofibers Fabricated by Modified Electrospinning and Centrifugal Jet Spinning Techniques. J. Nanosci. Nanotechnol. 2017, 17, 9056-9062.
- (10) Mirjalili, M.; Zohoori, S. Review for Application of Electrospinning and Electrospun Nanofibers Technology in Textile Industry. J. Nanostruct. Chem. 2016, 6, 207-213.
- (11) Pisignano, D. Polymer Nanofibers Building Blocks for Nanotechnology; The Royal Society of Chemistry: Thomas Graham House: Science Park, Milton Road, Cambridge CB4 0WF, UK, 2013.
- (12) Yang, M.; Cao, K.; Sui, L.; Qi, Y.; Zhu, J.; Waas, A.; Arruda, E. M.; Kieffer, J.; Thouless, M. D.; Kotov, N. A. Dispersions of Aramid Nanofibers: A New Nanoscale Building Block. ACS Nano 2011, 5, 6945-6954.
- (13) Shi, Q.; Vitchuli, N.; Nowak, J.; Jiang, S.; Caldwell, J. M.; Breidt, F.; Bourham, M.; Zhang, X.; McCord, M. Multifunctional and Durable Nanofiber-Fabric-Layered Composite for Protective Application. J. Appl. Polym. Sci. 2013, 128, 1219-1226.
- (14) Ryu, S.-Y.; Chung, J. W.; Kwak, S.-Y. Tunable multilayer assemblies of nanofibrous composite mats as permeable protective materials against chemical warfare agents. RSC Adv. 2017, 7, 9964-
- (15) Ying, W. B.; Kim, S.; Lee, M. W.; Go, N. Y.; Jung, H.; Ryu, S. G.; Lee, B.; Lee, K. J. Toward a Detoxification Fabric Against Nerve Gas Agents: Guanidine-Functionalized Poly[2-(3-butenyl)-2-oxazoline]/Nylon-6,6 Nanofibers. RSC Adv. 2017, 7, 15246-15254.
- (16) Liu, X.; Zhou, Y.; Zhang, J.; Tang, L.; Luo, L.; Zeng, G. Iron Containing Metal-Organic Frameworks: Structure, Synthesis, and Applications in Environmental Remediation. ACS Appl. Mater. Interfaces 2017, 9, 20255-20275.
- (17) Vellingiri, K.; Philip, L.; Kim, K.-H. Metal-organic Frameworks as Media for the Catalytic Degradation of Chemical Warfare Agents. Coord. Chem. Rev. 2017, 353, 159-179.
- (18) Wen, M.; Mori, K.; Kuwahara, Y.; An, T.; Yamashita, H. Design and Architecture of Metal Organic Frameworks for Visible Light Enhanced Hydrogen Production. Appl. Catal., B 2017, 218, 555-569.
- (19) Dhummakupt, E. S.; Carmany, D. O.; Mach, P. M.; Tovar, T. M.; Ploskonka, A. M.; Demond, P. S.; DeCoste, J. B.; Glaros, T. Metal-Organic Framework Modified Glass Substrate for Analysis of Highly Volatile Chemical Warfare Agents by Paper Spray Mass Spectrometry. ACS Appl. Mater. Interfaces 2018, 10, 8359-8365.
- (20) Gallis, D. F. S.; Harvey, J. A.; Pearce, C. J.; Hall, M. G.; DeCoste, J. B.; Kinnan, M. K.; Greathouse, J. A. Efficient MOF-based Degradation of Organophosphorus Compounds in Non-aqueous Environments. J. Mater. Chem. A 2018, 6, 3038-3045.
- (21) Liu, Y.; Howarth, A. J.; Vermeulen, N. A.; Moon, S.-Y.; Hupp, J. T.; Farha, O. K. Catalytic Degradation of Chemical Warfare Agents and their Simulants by Metal-organic Frameworks. Coord. Chem. Rev. 2017, 346, 101-111.
- (22) Momeni, M. R.; Cramer, C. J. Dual Role of Water in Heterogeneous Catalytic Hydrolysis of Sarin by Zirconium-Based Metal-Organic Frameworks. ACS Appl. Mater. Interfaces 2018, 10, 18435-18439.
- (23) Ploskonka, A. M.; DeCoste, J. B. Insight into Organophosphate Chemical Warfare Agent Simulant Hydrolysis in Metal-Organic Frameworks. J. Hazard. Mater. 2019, 375, 191-197.
- (24) Liang, H.; Yao, A.; Jiao, X.; Li, C.; Chen, D. Fast and Sustained Degradation of Chemical Warfare Agent Simulants Using Flexible

- Self-Supported Metal-Organic Framework Filters. ACS Appl. Mater. Interfaces 2018, 10, 20396–20403.
- (25) Yao, A.; Jiao, X.; Chen, D.; Li, C. Photothermally Enhanced Detoxification of Chemical Warfare Agent Simulants using Bioinspired Core-Shell Dopamine-Melanin@Metal-Organic Frameworks and Their Fabrics. ACS Appl. Mater. Interfaces 2019, 11, 7927–7935.
- (26) Shen, C.; Mao, Z.; Xu, H.; Zhang, L.; Zhong, Y.; Wang, B.; Feng, X.; Tao, C.-a.; Sui, X. Catalytic MOF-loaded cellulose sponge for rapid degradation of chemical warfare agents simulant. *Carbohydr. Polym.* **2019**, *213*, 184–191.
- (27) Dwyer, D. B.; Lee, D. T.; Boyer, S.; Bernier, W. E.; Parsons, G. N.; Jones, W. E. Toxic Organophosphate Hydrolysis Using Nanofiber-Templated UiO-66-NH2 Metal-Organic Framework Polycrystalline Cylinders. ACS Appl. Mater. Interfaces 2018, 10, 25794—25803.
- (28) Lee, D. T.; Zhao, J.; Oldham, C. J.; Peterson, G. W.; Parsons, G. N. UiO-66-NH2 Metal-Organic Framework (MOF) Nucleation on TiO2, ZnO, and Al2O3 Atomic Layer Deposition-Treated Polymer Fibers: Role of Metal Oxide on MOF Growth and Catalytic Hydrolysis of Chemical Warfare Agent Simulants. ACS Appl. Mater. Interfaces 2017, 9, 44847–44855.
- (29) Lee, D. T.; Zhao, J.; Peterson, G. W.; Parsons, G. N. Catalytic "MOF-Cloth" Formed via Directed Supramolecular Assembly of UiO-66-NH2 Crystals on Atomic Layer Deposition-Coated Textiles for Rapid Degradation of Chemical Warfare Agent Simulants. *Chem. Mater.* **2017**, 29, 4894–4903.
- (30) Lu, A. X.; McEntee, M.; Browe, M. A.; Hall, M. G.; DeCoste, J. B.; Peterson, G. W. MOFabric: Electrospun Nanofiber Mats from PVDF/UiO-66-NH2 for Chemical Protection and Decontamination. *ACS Appl. Mater. Interfaces* **2017**, *9*, 13632–13636.
- (31) McCarthy, D. L.; Liu, J.; Dwyer, D. B.; Troiano, J. L.; Boyer, S. M.; DeCoste, J. B.; Bernier, W. E.; Jones, W. E., Jr Electrospun Metal-Organic Framework Polymer Composites for the Catalytic Degradation of Methyl Paraoxon. *New J. Chem.* **2017**, *41*, 8748–8753.
- (32) Zhao, J.; Lee, D. T.; Yaga, R. W.; Hall, M. G.; Barton, H. F.; Woodward, I. R.; Oldham, C. J.; Walls, H. J.; Peterson, G. W.; Parsons, G. N. Ultra-Fast Degradation of Chemical Warfare Agents Using MOF-Nanofiber Kebabs. *Angew. Chem., Int. Ed.* **2016**, 55, 13224–13228.
- (33) Islamoglu, T.; Atilgan, A.; Moon, S.-Y.; Peterson, G. W.; DeCoste, J. B.; Hall, M.; Hupp, J. T.; Farha, O. K. Cerium(IV) vs Zirconium(IV) Based Metal-Organic Frameworks for Detoxification of a Nerve Agent. *Chem. Mater.* **2017**, *29*, 2672–2675.
- (34) Plonka, A. M.; Wang, Q.; Gordon, W. O.; Balboa, A.; Troya, D.; Guo, W.; Sharp, C. H.; Senanayake, S. D.; Morris, J. R.; Hill, C. L.; Frenkel, A. I. In Situ Probes of Capture and Decomposition of Chemical Warfare Agent Simulants by Zr-Based Metal Organic Frameworks. *J. Am. Chem. Soc.* **2017**, *139*, 599–602.
- (35) Bandosz, T. J.; Laskoski, M.; Mahle, J.; Mogilevsky, G.; Peterson, G. W.; Rossin, J. A.; Wagner, G. W. Reactions of VX, GD, and HD with Zr(OH)4: Near Instantaneous Decontamination of VX. *J. Phys. Chem. C* **2012**, *116*, 11606–11614.
- (36) Shigekawa, H.; Ishida, M.; Miyake, K.; Shioda, R.; Iijima, Y.; Imai, T.; Takahashi, H.; Sumaoka, J.; Komiyama, M. Extended X-ray Absorption Fine Structure Study on the Cerium(IV)-induced DNA Hydrolysis: Implication to the Roles of 4f Orbitals in the Catalysis. *Appl. Phys. Lett.* **1999**, *74*, 460–462.
- (37) Yuan, Y.; Kozlova, A. P.; Asakura, K.; Wan, H.; Tsai, K.; Iwasawa, Y. Supported Au Catalysts Prepared from Au Phosphine Complexes and As-Precipitated Metal Hydroxides: Characterization and Low-Temperature CO Oxidation. *J. Catal.* **1997**, *170*, 191–199.
- (38) Klet, R. C.; Liu, Y.; Wang, T. C.; Hupp, J. T.; Farha, O. K. Evaluation of Brønsted acidity and proton topology in Zr- and Hf-based metal-organic frameworks using potentiometric acid-base titration. J. Mater. Chem. A 2016, 4, 1479–1485.
- (39) Peterson, G. W.; Rossin, J. A.; Karwacki, C. J.; Glover, T. G. Surface Chemistry and Morphology of Zirconia Polymorphs and the Influence on Sulfur Dioxide Removal. *J. Phys. Chem. C* **2011**, *115*, 9644–9650.

- (40) Peterson, G. W.; Lu, A. X.; Epps, T. H. Tuning the Morphology and Activity of Electrospun Polystyrene/UiO-66-NH2 Metal-Organic Framework Composites to Enhance Chemical Warfare Agent Removal. ACS Appl. Mater. Interfaces 2017, 9, 32248–32254.
- (41) Katz, M. J.; Mondloch, J. E.; Totten, R. K.; Park, J. K.; Nguyen, S. T.; Farha, O. K.; Hupp, J. T. Simple and Compelling Biomimetic Metal-Organic Framework Catalyst for the Degradation of Nerve Agent Simulants. *Angew. Chem., Int. Ed.* **2014**, *53*, 497–501.
- (42) Dwyer, D. B.; Dugan, N.; Hoffman, N.; Cooke, D. J.; Hall, M. G.; Tovar, T. M.; Bernier, W. E.; DeCoste, J.; Pomerantz, N. L.; Jones, W. E. Chemical Protective Textiles of UiO-66-Integrated PVDF Composite Fibers with Rapid Heterogeneous Decontamination of Toxic Organophosphates. ACS Appl. Mater. Interfaces 2018, 10, 34585–34591.
- (43) Bhute, M. V.; Kondawar, S. B. Electrospun poly(vinylidene fluoride)/cellulose acetate/AgTiO2 nanofibers polymer electrolyte membrane for lithium ion battery. *Solid State Ionics* **2019**, 333, 38–44.
- (44) Kim, S.; Han, T.; Jeong, J.; Lee, H.; Ryou, M.-H.; Lee, Y. M. A Flame-Retardant Composite Polymer Electrolyte for Lithium-Ion Polymer Batteries. *Electrochim. Acta* **2017**, 241, 553–559.
- (45) Fang, L.-F.; Zhu, B.-K.; Zhu, L.-P.; Matsuyama, H.; Zhao, S. Structures and Antifouling Properties of Polyvinyl Chloride/poly-(methyl methacrylate)-graft-poly(ethylene glycol) Blend Membranes Formed in Different Coagulation Media. J. Membr. Sci. 2017, 524, 235–244.
- (46) Huang, S.; Ras, R. H. A.; Tian, X. Antifouling Membranes for Oily Wastewater Treatment: Interplay Between Wetting and Membrane Fouling. *Curr. Opin. Colloid Interface Sci.* **2018**, *36*, 90–109.
- (47) Li, Y.; Huang, S.; Zhou, S.; Fane, A. G.; Zhang, Y.; Zhao, S. Enhancing Water Permeability and Fouling Resistance of Polyvinylidene Fluoride Membranes with Carboxylated Nanodiamonds. *J. Membr. Sci.* **2018**, *556*, 154–163.
- (48) Liu, D.; Zhu, J.; Qiu, M.; He, C. Antifouling Performance of Poly(lysine methacrylamide)-grafted PVDF Microfiltration Membrane for Solute Separation. Sep. Purif. Technol. 2016, 171, 1–10.
- (49) Venault, A.; Huang, W.-Y.; Hsiao, S.-W.; Chinnathambi, A.; Alharbi, S. A.; Chen, H.; Zheng, J.; Chang, Y. Zwitterionic Modifications for Enhancing the Antifouling Properties of Poly-(vinylidene fluoride) Membranes. *Langmuir* **2016**, *32*, 4113–4124.
- (50) Boateng, B.; Zhu, G.; Lv, W.; Chen, D.; Feng, C.; Waqas, M.; Ali, S.; Wen, K.; He, W. An Efficient, Scalable Route to Robust PVDF-co -HFP/SiO2 Separator for Long-Cycle Lithium Ion Batteries. *Phys. Status Solidi RRL* **2018**, *12*, 1800319.
- (51) Li, J.; Luo, K.; Yu, J.; Wang, Y.; Zhu, J.; Hu, Z. Promising Free-Standing Polyimide Membrane via Solution Blow Spinning for High Performance Lithium-Ion Batteries. *Ind. Eng. Chem. Res.* **2018**, *57*, 12296–12305.
- (52) Liu, J.; Yang, K.; Mo, Y.; Wang, S.; Han, D.; Xiao, M.; Meng, Y. Highly Safe Lithium-ion Batteries: High Strength Separator from Polyformaldehyde/cellulose Nanofibers Blend. *J. Power Sources* **2018**, 400. 502–510.
- (53) Woodard, L. N.; Grunlan, M. A. Hydrolytic Degradation and Erosion of Polyester Biomaterials. *ACS Macro Lett.* **2018**, *7*, 976–982.
- (54) Venault, A.; Liou, C.-S.; Yeh, L.-C.; Jhong, J.-F.; Huang, J.; Chang, Y. Turning Expanded Poly(tetrafluoroethylene) Membranes into Potential Skin Wound Dressings by Grafting a Bioinert Epoxylated PEGMA Copolymer. *ACS Biomater. Sci. Eng.* **2017**, 3, 3338–3350.
- (55) Zander, Z. K.; Becker, M. L. Antimicrobial and Antifouling Strategies for Polymeric Medical Devices. *ACS Macro Lett.* **2018**, *7*, 16–25.